Molecular-dynamics study of energy flow and the Kapitza conductance across an interface with imperfection formed by two dielectric thin films

Cherng-Jyh Twu and Jeng-Rong Ho*
Department of Mechanical Engineering, National Chung Cheng University, Chia-Yi, Taiwan 621, Republic of China
(Received 26 August 2002; revised manuscript received 31 January 2003; published 28 May 2003)

A molecular-dynamics study of the flow of thermal and mechanical energies and the Kapitza conductance across both ideal and imperfect interfaces formed by two dielectric thin films is presented. The numerical experiments were achieved on a three-dimensional lattice configuration consisting of two kinds of fcc lattice particles having, respectively, Lennard-Jones and Morse interaction potentials. The degree of discrepancy between the two films was realized through altering the parameter of the interaction potential. Interfacial imperfections due to interdiffusion and a vacancy were considered. An effective computational procedure was proposed to release the initial stress induced by forming the two-layered structure. Results show that a large temperature jump occurred at the interface, and that the interfacial resistance dominated the effective conductivity of the whole film. Both the Kapitza conductance and the effective conductivity of the whole film decreased with the increase of the discrepancy between the two films, as well as decreased with the increase of the degree of disorder around the interface. With the increase of the system temperature, the temperature jump at the interface decreased and the Kapitza conductance increased. The effective conductivity, however, first increased then decreased with temperature. A peak conductivity was thus observed. The process of the energy transition for the pulsed, propagating elastic, and thermal energies, especially at the duration of passing through the interface, was demonstrated. The transmission coefficient of the energy through the interface was calculated, and the transformation of the energy from elastic to thermal was illustrated.

DOI: 10.1103/PhysRevB.67.205422 PACS number(s): 68.35.−p, 67.40.Pm, 66.70.+f, 63.22.+m

I. INTRODUCTION

Nowadays, due to the rapid progress in fabrication technology, a highly sophisticated, multilayered thin film structure is often employed for a particular purpose in today's state-of-the-art engineering systems. Energy transport at the interface between thin solid layers is thus not only of fundamental significance but also has a practical importance in determining the performance of many components and devices. Microscopically, the transfer of thermal and mechanical energies in materials is accomplished through movement of atoms. As the energy passes through an interface, the type of movement of the atoms may be significantly altered, and this sometimes results in a considerable change in property. One apparent example is when heat current is transported across an interface between two different materials; there will in general be a macroscopic temperature discontinuity at the interface. This effect, called the thermal resistance, was noticed as early as 1936.[1,2] Kapitza reported his measurements of the temperature drop at the interface between copper and liquid helium.[3] The Kapitza conductance, defined as $\sigma_k = \dot{Q}/(A\Delta T)$, can be employed to describe the effective macroscopic interfacial conductance. In the above expression, A is the area of the interface, ΔT is the temperature difference on the two sides of the interface, and $\dot{Q}$ is the heat flow across the interface. Theoretical estimations of the thermal resistance at the interface between two solids were based on the acoustic mismatched theory[4,5] and the diffuse mismatched theory.[6] The former assumed that phonons propagated as a plane wave, with a wavelength much larger than the interatomic spacings, and that the media were treated as continua. The latter, on the opposite extreme, assumed that all phonons were diffusively scattered at the interface, i.e., an incident phonon was reflected and transmitted into all phonon states with the same energy. A very informative study about thermal boundary resistance that included a very comprehensive literature review upto the late 1980s was reported by Swartz and Pohl.[7]

The theoretical models only work well for solid-solid interfaces at very low temperatures; however, they are not suitable for situations at high temperature. From the viewpoint of phonon transport, neither of the above mismatched theories takes the phonon dispersion effect, which becomes more crucial at high temperature, into account. The lattice-dynamical theory was thus employed to include these effects by several investigators.[8–10] Among these, Young and Maris presented a three-dimensional calculation of phonon transmission and the Kapitza conductance at the interface between two semi-infinite fcc lattices that had different masses and spring constants. They calculated the spectral density of the transmitted phonon flux, the spectral dependence of the phonon transmission coefficient, and the temperature dependence of boundary resistance. They found that the Kapitza resistance was proportional to T^3 at low temperatures and independent of T for temperatures larger than the Debye temperature θ_D. Pettersson and Mahan[11] extended the study to two bounded media with dissimilar lattice constants and allowed more phonons to be generated at the interface. The additional generated high-frequency phonons were found to be responsible for an appreciable amount of the reflected and transmitted heat. Introducing a scattering region between two identical semi-infinite leads of uniform cross section, Fagas *et al.*[12] studied the generic properties of elastic phonon transport by the method of lattice dynamics. They found that phonon transmittance is a strong function of the frequency and

the disorder correlation length.

Several experimental studies of the interfacial resistance were also very notable.[13–15] Creating a suitable interface condition and making a noninvasive measurement for the ultrathin film structure, however, present new challenges to experimental study. Another powerful tool to study the interfacial phenomena is the molecular dynamics (MD) simulation. With the improvement of the accuracy of the potential functions for molecules and the rapid progress of the computer power, MD has demonstrated its great potential in phenomena for materials with complicated structures[16] Ikeshoji and Hafskjold[17] presented an algorithm for nonequilibrium molecular dynamics to study heat conduction in liquids and through a liquid-gas interface. They showed the size effect on thermal conductivity in a liquid state and observed a clear temperature jump between the liquid-vapor interface. Maiti *et al.*[18] studied heat flow and the Kapitza resistance across grain boundaries of crystalline Si using MD simulations. Their results showed that Fourier's law was valid even under large temperature gradients, 1 K per Å, and there was a dramatic temperature jump across interface of different crystals. Lukes *et al.*[19] used MD to predict the thermal conductivity of a solid argon thin film in the direction perpendicular to the film plane. Their calculations showed that the thermal conductivity at all temperatures increases with film thickness, and that thin-film size effects were more pronounced at lower temperatures. More recently, MD had also been used to study the thermal conductivity for a superlattice structure where the phonon-based model is complex and the energy transfer at interfaces remains unclear.[20–22]

The above review indicates that previous theoretical works on the Kapitza resistance were mainly based on the assumption of an ideal interface formed by two semi-infinite structures at low temperatures, while studies by MD simulations were also for an ideal interface but included the solid-liquid interface. Works that incorporated the effect of imperfections were also limited for semi-infinite structures. No results, to the authors' best knowledge, showing the process of the energy transition, especially at the duration of passing through an interface, are available. This study employs the MD method because, in MD, incorporating the effect of interfacial imperfections and observing the process of energy transition are very straightforward and the influence of thermal fluctuations on phonon scattering is included naturally. The present work studies the Kapitza conductance and the effective conductivity of a two-layered structure formed by different dielectric thin films. Dependences of the conductance on the discrepancy of the two materials as well as on the temperature are studied. Effects of the interface imperfection, due to interdiffusion and the vacancy, on the Kapitza conductance and the effective conductivity are also presented. The transformation of energy from kinetic into thermal is examined. Transmission coefficients for elastic and thermal energies through interface are also calculated.

II. PHYSICAL MODEL AND SIMULATION METHOD

In order to study the interfacial properties and observe the transition of energy across an interface, we constructed a three-dimensional lattice structure formed by two dielectric thin films, shown in Fig. 1, that was made up of two different types of atoms: *A* on the left side and *B* on the right side, respectively. Hereafter we call these films *A* and *B*. A physical interface was naturally formed at their junction. Atoms in film *A* were assumed to interact with each other through the Lennard-Jones (12-6) pair interaction potentials of the form $\Phi_{\mathrm{LJ}}=4\varepsilon[(\sigma/R_{ij})^{12}-(\sigma/R_{ij})^{6}]$, where the subscript *ij* represents the connection between pair atoms *i* and *j*, R_{ij} is the distance between the pair atoms to be considered, and the parameters ε and σ, providing the scale of energy and distance, represent the bonding energy and equilibrium separation distance between the pair atoms, respectively. For the convenience of a description and reduction of the potential computational roundoff error, we selected the energy scale ε, length scale σ, and the atomic mass scale *m* of the argon atom to nondimensionalize all subsequent expressions. The dimensionless Lennard-Jones potential function was thus given as

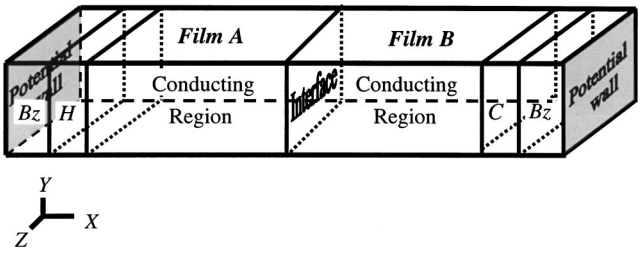

FIG. 1. Schematic diagram showing the lattice configuration and indicating the terms used in this study.

$$\phi_{\mathrm{LJ}}(r_{ij})=4[r_{ij}^{-12}-r_{ij}^{-6}], \tag{1}$$

and the resulting units for time, temperature, velocity, force, and stress are $t/\sigma\sqrt{m/\varepsilon}$, k_BT/ε, $v/\sqrt{\varepsilon/m}$, $f/(\varepsilon/\sigma)$, and $s/(\varepsilon/\sigma^3)$, respectively. Quantities presented in this study are all dimensionless. The atomic interaction potential for film *B* was described by the Morse potential given as

$$\phi_M(r_{ij})=d\{\exp[-2\beta(r_{ij}-r_0)]-2\exp[-\beta(r_{ij}-r_0)]\}. \tag{2}$$

In this expression, *d* and β denote, respectively, the depth and width of the potential, while r_0 is the distance that corresponds to the minimum energy on the potential well.

Sketched in Fig. 1, the geometry of the considered model was made up of (100) fcc lattices that consisted of 60 unit cells in the longitudinal direction *x*, and of five unit cells in the transverse directions *y* and *z*. The dimensionless lattice constant of the lattice, *a*, was $\sqrt{2}$, the density of the system was at $\sqrt{2}$, and totally 6000 atoms were involved in computations. Except for the consideration of the temperature dependence, the system temperature was set at $\frac{1}{3}$. To prevent the boundary effect in transverse directions, periodic boundary conditions were used in both *y* and *z* directions. Thus the interface could be regarded as a border formed by two infinite thin films. In the *x* direction, one additional surface layer, represented by Potential wall in Fig. 1, composed of Lennard-Jones atoms was put on both ends, at $x=-0.5$ and

$60a+0.5$. These atoms interacted only in the x direction with the atoms in the computational region through the interaction potential described by Eq. (1). To calculate the desired transport phenomena at the interface, we divided the computational region for each thin film into three zones, from the end toward the interface, the buffer zone (*Bz*, in Fig. 1), the temperature control zone (*H* or *C*, in Fig. 1), and the conduction zone. The buffer zone, with width of $2a$, was for the purpose of connecting the boundary and the temperature control zone. The temperature control zone, of thickness $3a$, was designed to provide the required thermal conditions for the conduction zone. The HLME method[23–25] was employed to rule the atoms in the temperature control zone at the desired kinetic temperature, T_{KE}, which is defined as

$$T_{KE}=\frac{1}{3\mathcal{N}}\sum_{i=1}^{\mathcal{N}} v_i^2, \tag{3}$$

where $\mathcal{N}$ was the number of atoms that were used to evaluate the local temperature. $\mathcal{N}$ was 300 for the temperature control zone and 100 for the conduction zone. The temperature was defined as

$$T=\frac{1}{3\mathcal{N}}\sum_{i}^{\mathcal{N}} (\mathbf{v}_i-\overline{\mathbf{v}})^2 \quad \text{where } \overline{\mathbf{v}}=\frac{1}{\mathcal{N}}\sum_{i=1}^{\mathcal{N}} \mathbf{v}_i . \tag{4}$$

These two expressions show that the two temperatures agree with each other at thermal equilibrium for solids.

The thickness of each conduction zone was $25a$, where each atom obeyed Newton's second law of motion. The heat flux was calculated according to

$$\mathbf{q}=\frac{1}{\mathcal{V}}\left\{\sum_{i=1}^{\mathcal{N}}\left[\mathbf{v}_i E_i+\frac{1}{2}\sum_{j=1,j\neq i}^{\mathcal{N}} \mathbf{r}_{ij}(\mathbf{F}_{ij}\cdot\mathbf{v}_i)\right]\right\}, \tag{5}$$

where $\mathcal{V}$ was the volume occupied by the $\mathcal{N}$ considered atoms, $\mathbf{F}_{ij}$ was the interaction force between atoms i and j, $\mathbf{r}_{ij}=\mathbf{r}_i-\mathbf{r}_j$, and, $E_i=\frac{1}{2}[m_i v_i^2+\Sigma_{j=1,j\neq i}^{\mathcal{N}}\phi(r_{ij})]$ was the energy of the atom i. The interaction potential between the two different types of atom A and B was assumed through the Lennard-Jones potential of

$$\phi_I(r_{ij})=4\left[\left(\frac{\sigma_I}{r_{ij}}\right)^{12}-\left(\frac{\sigma_I}{r_{ij}}\right)^{6}\right], \tag{6}$$

where σ_I was the mathematical mean of the equilibrium distances of the *A*-*A* and *B*-*B* atoms, and was equal to $(1+r_0)/2$.

We assumed that both the mass and depth of the potential of the two considered atoms were unitary. The degree of discrepancy between the two materials was accomplished by tuning the width of the potential for *B* atoms, the parameter β in Eq. (2). With the change of β, the properties of film *B* were changed and so was the state of the interface. To describe more quantitatively the degree of the discrepancy between the two materials, a parameter g, defined as $g=W_M/W_{\mathrm{LJ}}$, was employed as a free parameter in this study. W was the width of the potential when ϕ was at its half value ($\phi=-\frac{1}{2}$ in the dimensionless system). Numerical values of W for both types of atoms, with the Lennard-Jones potential and the Morse potential, were $W_{\mathrm{LJ}}=0.35$ and $W_M=1.76275/\beta$, respectively. Six values of g, 1.0, 1.1, 1.3, 1.6, 1.8, and 2.0, were used in this study. A schematic diagram showing W and g is shown in Fig. 2 and numerical values for variables in Morse potential at different *gs* are presented in Table 1. r_c in the table represents the cut off distance.

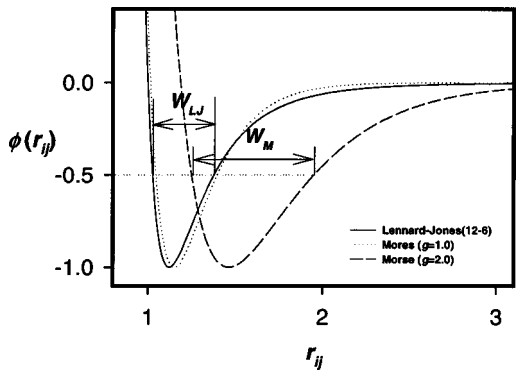

FIG. 2. Diagram showing Lennard-Jones and Morse potentials as functions of the atomic separation. The definitions of W for the two potentials are schematically presented and the effect of g on the potential function is also illustrated.

Initially a random kinetic energy drawn from a Boltzmann distribution, subjected to the desired system temperature, was first assigned to each atom in the computational region. Then the atomic spacing and the whole computational domain must be readjusted to release the initial stress. An initial stress free sample was crucial to the computational results, especially to phenomena and properties at an interface where different materials were joined. In this study, the stress was released as follows: first, the equilibrium interatomic distance between *B* atoms, r_0, was adjusted until the stresses on each end of the computational domain were the same; subsequently, the corresponding parameter of the set r_0 of *B* atoms were determined; finally, a stress-free, thermal equilibrium sample was achieved by modifying the amount of the average local momentum to be zero at every ten time steps. These procedures proved to be very effective. The initial stress introduced due to junction of the different materials could easily be released after 40 000 time steps at most. Figure 3 is an example showing the initial distributions of stresses and temperature in the computational domain at $g=1.3$ and $T=\frac{1}{3}$. Because of the symmetry in the y and z directions, the shear stress was very close to zero and the normal stress at each location varied around 62.2, the value

TABLE I. Numerical values for parameters in the Morse potential for different values of g. The initial samples were stress free and at thermal equilibrium. r_C is the cutoff distance.

g	1.0	1.1	1.3	1.6	1.8	2.0
β	5.027236	4.570214	3.867105	3.142022	2.792909	2.513618
r_0	1.1520	1.1775	1.2320	1.3253	1.3901	1.4623
r_C	2.5	2.5	2.5	3.0	3.0	3.5

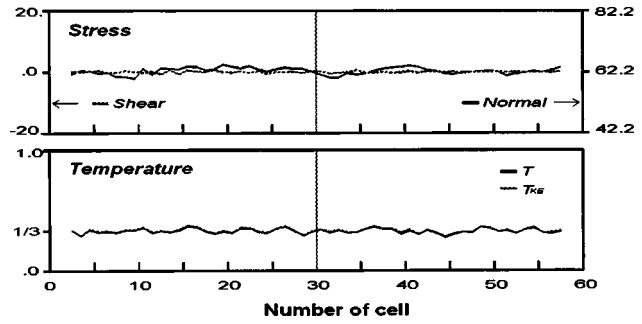

FIG. 3. Diagrams showing the initial stress and temperature distributions in the computational domain for the sample at $T=\frac{1}{3}$ and $g=1.3$.

of the preset system pressure. The close agreement between T_{KE} and T indicated that sample was in good thermal equilibrium.

The Kapitza conductance was calculated as follows: first, the steady temperature distributions $T_1(x)$ and $T_2(x)$ (see Fig. 4) were obtained; then, the temperature jump at interface ΔT_{int} was calculated as $\Delta T_{\text{int}}=T_1(1/2L_x)-T_2(1/2L_x)$; the Kapitza conductance was finally calculated as $\sigma_k=q_X/\Delta T_{\text{int}}$. Here $q_X=(q_{X1}+q_{X2})/2$, q_{X1}, and q_{X2} were the average heat fluxes in the two conduction zones. The effective conductivity of the whole structure was calculated as $\lambda_e=[(L_X/2)q_X/\Delta T_{\text{eff}}]$, where $\Delta T_{\text{eff}}=T_1(\frac{1}{4}L_X)-T_2(\frac{3}{4}L_X)$. L_X in the above expressions represented the length of the computational domain that was equal to $60a$. Resisivities for films A and B were calculated as the temperature difference divided by the heat flux, and for interface was found by $1/A\sigma_k$.

III. RESULTS AND DISCUSSION

Once the thermal equilibrium, stress-free sample was established, the temperature gradient was then set up by assigning the high and low temperatures on the temperature control zones, H and C in Fig. 1. Newton's law of motion was numerically integrated for each atom using a fifth-order Gear predictor-corrector algorithm with a time step of 6.0×10^{-4}. The static interfacial properties were then calculated as the steady state was achieved. Figure 5 shows the Kapitza

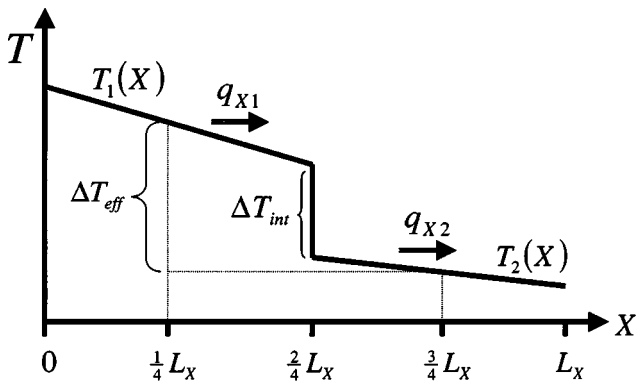

FIG. 4. Schematic diagram demonstrating terms that are used to calculate material properties in this study.

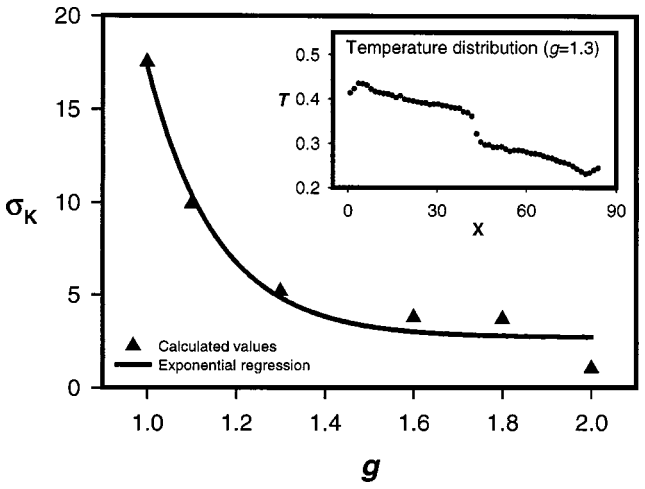

FIG. 5. Diagram showing the Kapitza conductance as a function of g at $T=\frac{1}{3}$. The inserted diagram presents the temperature distribution in the computational region for $g=1.3$. A large temperature drop at the interface can be observed.

conductance σ_k as a function of the parameter g when the temperature difference between the hot and cold zones was 0.2. With an increase of the discrepancy, one aspect of the parameter g of the two materials, the thermal resistance, increased monotonically. From the viewpoint of phonon transport, with the increase of the discrepancy on the two sides of the interface, more phonons would be reflected from the interface. The temperature distribution as a function of x for $g=1.3$ is presented in Fig. 5. It is shown that the temperature is distributed quite linearly in both films A and B and a clear temperature jump of $\Delta T_{\text{int}}=0.068$ was observed at the interface. This calculation showed that about 34% of temperature jump was occurred at interface.

The influence of g on the conductivity is further dis-

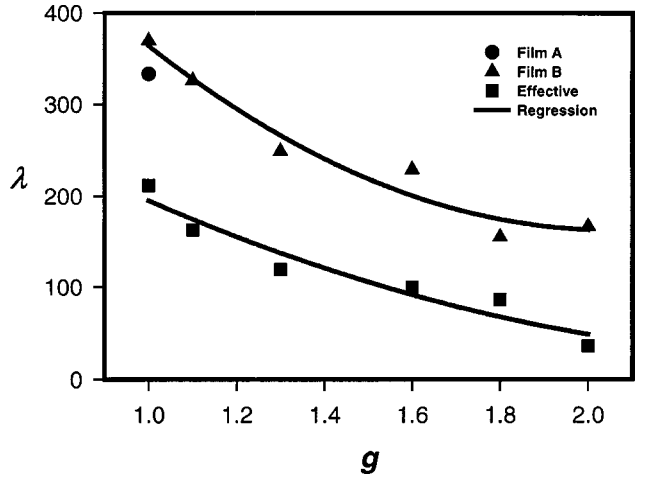

FIG. 6. Diagram showing the conductivity of the whole thin film as a function of g at $T=\frac{1}{3}$. The triangular points represent the conductivities as the whole film is formed solely from B atoms. The circle point is the conductivity if the film is made up by A atoms alone. The rectangular points illustrate conductivities of the two-layered thin film.

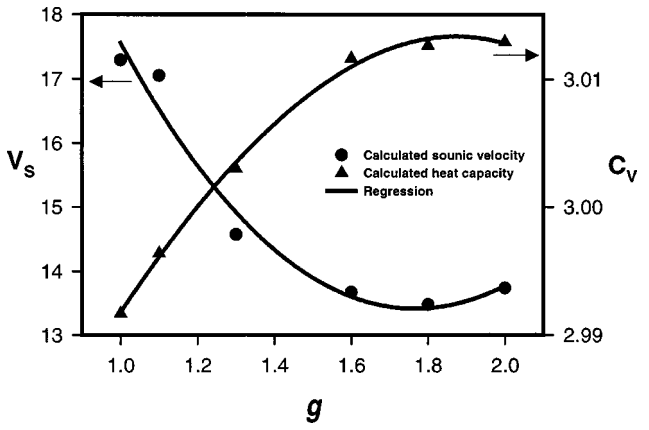

FIG. 7. Diagrams showing the dependences of the sonic velocity and the heat capacity upon g at $T=\frac{1}{3}$ when the whole film is formed solely from B atoms.

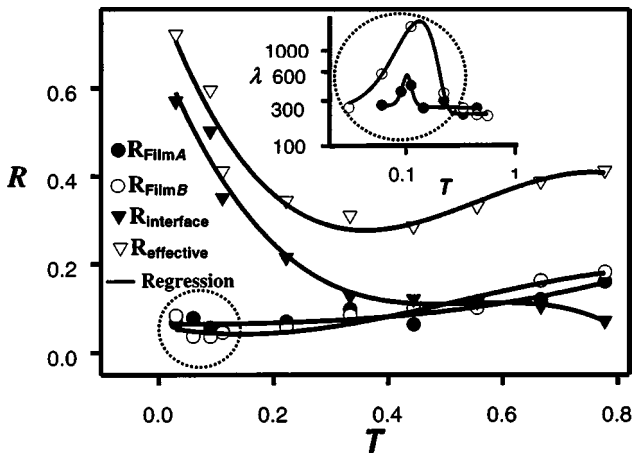

FIG. 8. Diagram showing the resistivities for the film A film B interface, and the effective resistivity of the whole film as a function of temperature at $g=1.3$. Conductances for films A and B at the low temperature region, indicated by the dashed circle, are presented as an inset.

cussed. In Fig. 6 the triangular points represent the thermal conductivity as a function of g when the whole thin film structure is formed only from B atoms. The circle point was the conductivity as the whole film was made solely from A atoms. When film A, with its state fixed at the state of the circle point, was ideally bonded with film B at different g's, the resulting effective conductivities of the whole thin film were represented by the rectangular points. It is shown that the thermal conductivity of the thin film, when formed from B atoms, decreases gradually with the increase of g. The theory of lattice dynamics indicates $\lambda \propto l C_v v_s$, where C_v is the specific heat per unit volume, v_s is the speed of phonon, and l is the phonon's mean free path.[26] The mean free path was mainly dependent on the temperature. Here the system temperature was fixed; thus only variations of v_s and C_v on g were considered. Figure 7 shows the dependences of v_s and C_v on g. Results indicated that C_v increased relatively slightly with g while v_s decreased more rapidly with g. Therefore, the trend of the dependence of λ on g was similar to the dependence of v_s on g. From the viewpoint of the potential function, an increase of g implies an increase of the width of the potential well (see Fig. 2), that results in an augmentation of each atom's effective distance as well as a decrease of the lattice elasticity. The former is related to the increase of C_v while the latter corresponds to the decrease of sonic velocity. Since both the interfacial conductance (in Fig. 5) and film B were decreased with the increase of g (Fig. 6 depicts the effective thermal conductivity), the rectangular points of the whole film decreased with the increase of g. It is noted that at $g=1$, a reduction of about 40% in the thermal conductivity arose due to the formation of the interface. Thus, it is the resistance at the interface that dominates conductance of the whole film.

Figure 8 shows the dependence of resistivities for the film A film B interface, and the effective value of the whole thin film structure as a function of temperature. Both dielectric films A and B show an increase of resistivity as the temperature is increased, except in the low temperature region indicated by the dotted circle. To highlight this region where thermal resistivities are small, the corresponding conductivity as a function of temperature is presented as an inset in the same figure. λ_{peak} is observable for each film. From the viewpoint of phonon transport,[27] for nonmetal materials $\lambda \propto T^3$ at low temperature, $T<\theta_D$, and $\lambda \propto T^1$ at high temperature, $T\sim\theta_D$ or larger; thus there will be a peak value of λ at a temperature smaller than θ_D on the λ-T plot. The Debye temperature for the present dimensionless system was expressed as $\theta_D=0.02946\times v_s(6\pi^2 n_d)^{1/3}$, where v_s was the sonic speed and $n_d=N/V$. The calculated θ_D was about 2.3. These calculations indicate the λ_{peak} also exists in ultrathin dielectric films.[28] Shown in Fig. 8, the interface resistivity $R_{\text{interface}}$ decreases first more rapidly then more slowly with the increase of temperature. The trend of the dependence of Kapitza conductance upon temperature is simply the inverse of the interface resistivity ($R_{\text{interface}}=1/A\sigma_k$). Our calculations also indicated that with an increase of the system temperature the temperature jump at the interface were gradually reduced and the interface became more and more ambiguous. The interface was almost indistinguishable as the system temperature was close to the phase transition temperature. Figure 8 shows that the effective resistivity $R_{\text{effective}}$ first decreased with the increase of temperature, reached a minimum, and then increased with a further increase of temperature. The effective resistivity was simply the superposition of each individual resistivity, i.e., $R_{\text{effective}}=R_{\text{Film}A}+R_{\text{Film}B}+R_{\text{interface}}$. At the low temperature region the resistance of the whole film was mainly contributed by the resistance at the interface; thus $R_{\text{effective}}$ presented the same trend of temperature dependence as $R_{\text{interface}}$. With an increase of temperature, the influence of the interface was reduced and resistances from both films were increased, this resulted in the increase of $R_{\text{effective}}$.

In a solid structure an interface can be formed by a contact or bond of two different materials or by different atomic structures in the same material. In the preceding discussions we assumed that the junction of films A and B formed a perfect interface. In real situations some interfacial imperfections, such as defects, voids, interdiffusion, and dislocation, possibly caused by differences in the atomic lattice constant,

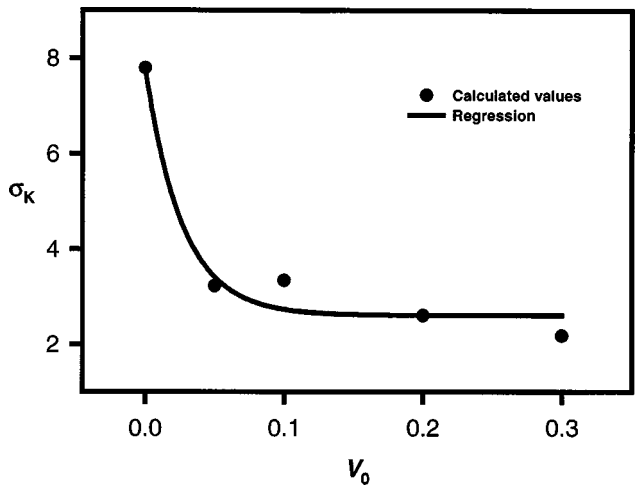

FIG. 9. Diagram showing the dependence of the Kapitza conductance upon the degree of the vacancy. The system temperature was $\frac{1}{3}$ and $g=1.3$.

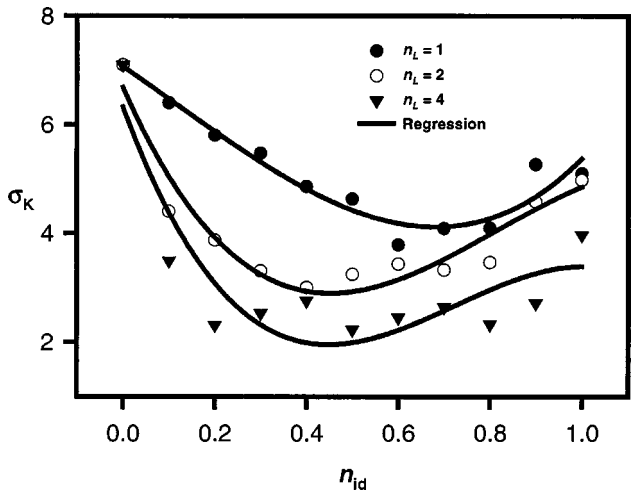

FIG. 10. Diagram showing the dependence of the Kapitza conductance as a function of the degree of the interdiffusion for different thicknesses of the interdiffused region. The system temperature was $\frac{1}{3}$, and $g=1.3$.

the chemical potential of the constituents, or from variations of the fabrication process or ambient temperature, may exist around the interface. In what follows imperfections due to interdiffusion and vacancy will be studied and discussed. The influence of a vacancy on the thermal resistance was studied by arbitrarily taking M atoms away from the interface. An index $V_o=M/M_i$ was defined to represent the degree of vacancy. Here M_i is total number of atoms on the two atomic planes forming the interface. Figure 9 indicates that the Kapitza conductance decreased monotonically with the increase of V_o. Vacancies on the interface reduce the number of passageway for phonon transport, and thus reduce the thermal conductivity. The vacancy can also be regarded as an impurity that, from the viewpoint of phonon transport, introduces additional obstacles to the scatter phonon and leads to an increase of the resistance.

To discuss the effect of interdiffusion on the thermal conductivity, we defined another parameter, called the index of the interfacial inter-diffusivity as $n_{id}=N_d/N_{\max}$. N_d is the number of atoms interchanged while $N_{\max}$ is the total number of atoms of the considered atomic layers that are allowed to interchange. Therefore, $n_{id}=0$ means a perfect interface without any interdiffusion $n_{id}=1$ represents a state of total exchange, and $n_{id}=0.5$ means that 50% of atoms in the considered interchangeable layers were exchanged, corresponding to the most disordered state around the interfacial region. Figure 10 shows the Kapitza conductance as a function of n_{id} when g was fixed at 1.3. In Fig. 10 n_L indicates the number of atomic layers (atomic planes) on each side of the interface that atoms were allowed to interchange with each other. Thus n_L can be regarded as an indication of the thickness of the interdiffused region. Generally, σ_κ first decreased gradually with the increase of n_{id} from $n_{id}=0$, reached its minimum around $n_{id}=0.5$, and increased progressively again until $n_{id}=1$. But the values of σ_κ around $n_{id}=1$ were lower than those around $n_{id}=0$. As the phonon reached the vicinity of the interface, the extra disorder due to interdiffusion introduced additional phonon scattering, and thus increased the resistance to phonon transport. With the increase of the atom interdiffusion, the degree of atomic disorder around the interface was increased and the maximum disorder state was around $n_{id}=0.5$, corresponding to the section of the lower thermal conductivity. When n_{id} was larger than 0.5, although the number of interdiffused atoms was increased, the degree of disorder decreased. As n_{id} was increased to 1, the interfacial region can be regarded as a region composed of three ideal interfaces; this explains why the value of σ_κ at $n_{id}=1$ was smaller than that at $n_{id}=0$. Figure 10 also shows that σ_κ decreases with an increase of the interdiffused region, n_L.

For a better understanding of the process of the energy transition, we created both ideal elastic and thermal energy pulses close to the interface in film A, and observed the evolution of their propagation. The ideal thermal energy pulse was generated by suddenly promoting atoms on the plane around $x=25a$ to a new equilibrium velocity distribution,[29] while an elastic energy pulse was created around $x=25a$ by moving all atoms for $x<25a$ in a rigid-body manner instantaneously a very small distance to the right. When the atoms around the perturbed plane were disturbed through the atomic interaction potentials, this disturbance first affected mainly atoms close to the perturbed region and then propagated in both directions along the x axis, due to the periodic boundary conditions in the y and z directions. As an elastic energy pulse was imposed, distributions of T_{KE} and T in the computational regions at several times for an imperfect interface with $n_L=4$, $n_{id}=0.5$ and $g=1.3$ are shown in Fig. 11. As defined by Eqs. (3) and (4), the departure of T_{KE} from T was contributed by the elastic energy. Thus the propagation of elastic and thermal energies could be observed from Fig. 11. At $t=100\Delta t$, temperature pulses of T_{KE} and T around $x=25a$ were observed. Part of the imposed elastic energy was transferred into the thermal energy, which was not diffused out far. At $t=300\Delta t$, a separation of the elastic wave into two parts that propagated in opposite directions were observed. The leftward part propagated at the sonic speed of

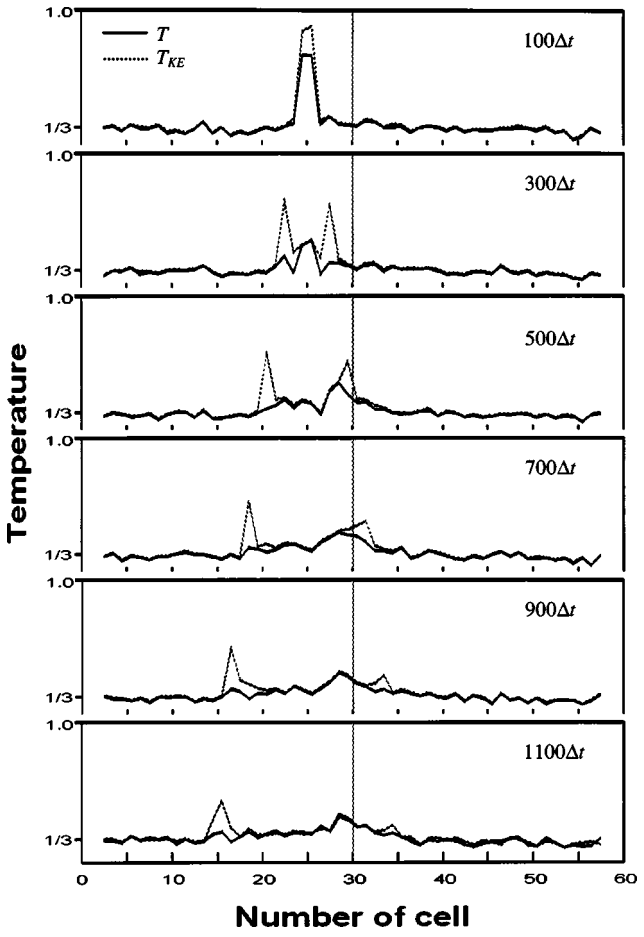

FIG. 11. Panels showing the distributions of temperatures T and T_{KE} in the computational domain for different times when an elastic energy pulse was imposed at $x=25a$ at $t=0$. The interface was imperfect with $n_L=4$ and $n_{id}=0$. The system temperature was $\frac{1}{3}$, and $g=1.3$.

film A and its amplitude was gradually reduced. This indicated, during its propagation, that the elastic energy was kept over a longer period from being transformed into the disordered thermal energy. The rightward wave penetrated the interface and propagated into film B. The interfacial resistance augmented by interdiffuse enhanced phonon scattering helped to transform more elastic energy into thermal energy. At $t=500\Delta t$ temperature, T on the left side of the interface was clearly enhanced, and the difference between T_{KE} and T was smaller than on the leftward one wave. The rightward wave kept penetrating the interfacial region and T_{KE} and T became close at $t=700\Delta t$. At $t=900\Delta t$ the rightward wave passed the interface, and much thermal energy was accumulated around the interfacial region. At $t=1100\Delta t$, most of the rightward elastic energy was transformed into thermal energy and became more indistinguishable, while the leftward elastic energy still could be identified clearly.

The transmission coefficient α for both elastic and thermal energies passing through the imperfect interface described in the previous paragraph were calculated and discussed. As described in the preceding paragraph, only about a half of the imposed elastic energy in film A propagated to

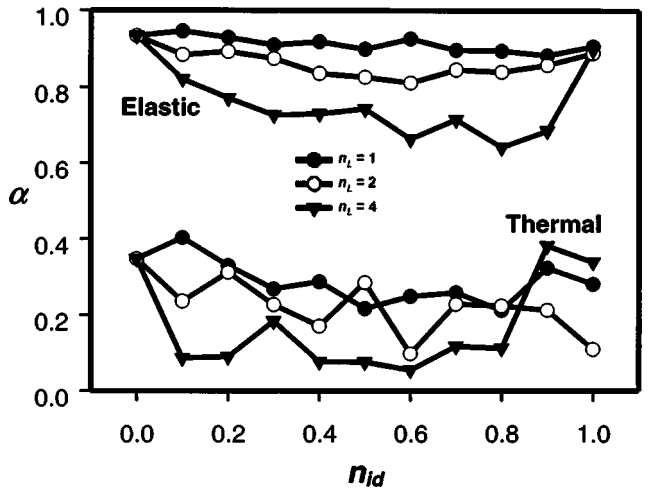

FIG. 12. Diagram showing the dependence of the transmission coefficient upon the degree of the interdiffusion for different thicknesses of the interdiffused region. The system temperature was $\frac{1}{3}$, and $g=1.3$.

the right and penetrated the interface. Once the elastic wave passed through the interface, α was defined as the total energy increased in film B divided by half of the initially applied elastic energy. The calculation of α for the thermal energy was different from that for the elastic energy because thermal energy was transferred through diffusion and a clear identification of the ending time of the transmission was difficult. Here α for the thermal energy was calculated as the averaged total energy increased in film B as $t=(4500-5000)\Delta t$ divided by half of the initial imposed thermal energy in film A. For the elastic energy, Fig. 12 shows that α was close to unitary and its variation with n_{id} was slight when $n_L=1$. As n_L was increased to 4, however, the effect of the interface on α was obvious, and its variation with n_{id} was significant. The elastic energy is a kind of energy expressed by the collective behavior of atoms that propagate through the lattice wave. If the range of the interfacial region was small, the longitudinal vibration wave was disturbed slightly and the elastic energy penetrated with only minor dissipation. As the interfacial region was enlarged, either its perturbation of the behavior of the collective, longitudinal, harmonic vibration was considerable, else the phonon scattering due to the interdiffused atoms in the interfacial region was substantial, and resulted in a lowering of the transmission coefficient. When a thermal energy was transmitted into the same interfacial region, Fig. 12 shows that the values of α were much smaller. Because the transfer of the thermal energy is due to phonons that travel randomly in all directions, the more disordered the interfacial region the more strongly phonon scattering would happen; in addition more thermal energy was blocked around the interface, that led to the smaller transmission coefficient. As time elapsed, however, the accumulated thermal energy at the interfacial region would be gradually diffused out until a new thermal equilibrium was reached.

IV. CONCLUSIONS

In this study, the interfacial conductance and both thermal and mechanical energy flows through an interface formed by

two dielectric thin films were studied by a molecular dynamics simulation. All numerical experiments were performed on a three-dimensional, filamentlike, lattice configuration consisting of fcc lattice particles. Two types of lattice particles were employed to represent the two considered dielectric thin films. One was the Lennard-Jones (12-6) interaction potential and the other was the Morse interaction potential. The degree of material discrepancy between the two films was realized by altering the parameter in the Morse potential. Interfacial defects due to interdiffusion and a vacancy were considered. Computational results were obtained by executing the law of motion for the 6000 atoms constituting the computational region. Initial stresses among the lattice particles induced by bonding the two films together were released by successively regulating the local averaged momentum to be zero. Law of motion for each atom was integrated by the fifth-order Gear prediction-corrector algorithm with numerical time steps of 6.0×10^{-4}. The effects of the atomic discrepancy, interfacial defect, and temperature upon the Kapitza conductance, as well as upon the effective conductivity of the whole film, were presented and discussed. Propagation of thermal and elastic energy pulses was observed and the transition of energy was examined. The major conclusions of this study are drawn as follows.

(1) At lower temperatures more than one third of the temperature jump would occur at the interface. This jump decreases with the increase of the system temperature. It is the resistance at the interface that dominates the effective conductivity of the whole thin film structure.

(2) Both the Kapitza conductance at the interface and the effective conductivity of the whole film decrease with the increase of the discrepancy between the two films as well as with the thickness of the defect and the degree of disorder at the interfacial region.

(3) With the increase of the system temperature, the effective resistance first decreases and then increases. The first decrease is due to the reduction of the resistance at the interface, while the increase is contributed by an enhancement of the resistance of each film. A maximum conductance λ_{peak} thus occurs on the λ-T plot for the two-layered thin film structure.

(4) As an elastic energy is propagating through an ideal interface formed by two thin films with close lattice constants, most of the energy penetrates with only a little dissipation. However, the degree of the transmission decreases with the increase of the discrepancy between the two films as well as the thickness and the degree of disorder at the interfacial region. If the energy is thermal, the degree of transmission is much smaller.

(5) The process of energy transition at the interface can be observed by the current molecular dynamics simulation method.

ACKNOWLEDGMENTS

Support for this work by the National Science Counsel of the Republic of China under Grant No. NSC90-2212-E-194-030 is gratefully acknowledged.

*Associate Professor, author to whom correspondence should be addressed. Mailing address: Department of Mechanical Engineering, National Chung Cheng University, Chia-Yi, Taiwan 621, Republic of China. FAX: +886-5-2720589. Electronic address: imejrho@ccu.edu.tw

[1] N. Kürti, B. V. Rollin, and F. Simon, Physica (Amsterdam) **3**, 266 (1936).
[2] W. H. Keesom and A. P. Keesom, Physica (Amsterdam) **3**, 359 (1936).
[3] P. L. Kapitza, J. Phys. USSR **4**, 181 (1941).
[4] I. M. Khalatniko, Zh. Eksp. Teor. Fiz. **22**, 687 (1952).
[5] W. A. Little, Can. J. Phys. **37**, 334 (1959).
[6] E. T. Swartz and R. O. Pohl, Appl. Phys. Lett. **51**, 200 (1987).
[7] E. T. Swartz and R. O. Pohl, Rev. Mod. Phys. **61**, 605 (1989).
[8] M. E. Lumpkin, W. M. Saslow, and W. M. Visscher, Phys. Rev. B **17**, 4295 (1978).
[9] B. V. Paranjape, N. Arimitsu, and E. S. krebes, J. Appl. Phys. **61**, 888 (1987).
[10] D. A. Young and H. J. Maris, Phys. Rev. B **40**, 3685 (1989).
[11] S. Pettersson and G. D. Mahan, Phys. Rev. B **42**, 7386 (1990).
[12] G. Fagas, A. G. Kozorezov, C. J. Lambert, and J. K. Wigmore, A. Peacock, A. Poelaert, and R. den Hartong, Phys. Rev. B **60**, 6459 (1999).
[13] D. A. Young, C. Thomsen, H. T. Grahn, H. J. Maris, and J. Tauc, *Phonon Scattering in Condensed Matter* (Springer, Berlin, 1986), pp. 49–51.
[14] R. J. Stoner and H. J. Maris, Phys. Rev. B **48**, 16 373 (1993).
[15] G. Chen, C. L. Tien, X. Wu, and J. S. Smith, J. Heat Transfer **116**, 325 (1994).
[16] A. Nakano, M. E. Bachlechner, P. Branicio, T. J. Campbell, I. Ebbsjö, R. K. Kalia, A. Madhukar, S. Ogata, A. Omeltchenko, J. P. Rino, F. Shimojo, P. Walsh, and P. Vashishta, IEEE Trans. Electron Devices **47**, 1084 (2000).
[17] T. Ikeshoji and B. Hafskjold, Mol. Phys. **81**, 251 (1994).
[18] A. Maiti, G. D. Mahan, and S. T. Pantelides, Solid State Commun. **102**, 517 (1997).
[19] J. R. Lukes, D. Li, X. G. Liang, and C. L. Tien, J. Heat Transfer **122**, 536 (2000).
[20] X. G. Liang and B. Shi, Mater. Sci. Eng., A **292**, 198 (2000).
[21] S. Volz, J. B. Saulnier, G. Chen, and P. Beauchamp, High Temp.-High Press. **32**, 709 (2000).
[22] S. Volz, J. B. Saulnier, G. Chen, and P. Beauchamp, Microelectron. J. **31**, 815 (2000).
[23] W. G. Hoover, A. J. C. Laad, and B. Moran, Phys. Rev. Lett. **48**, 1818 (1982).
[24] A. J. C. Ladd and W. G. Hoover, Phys. Rev. B **28**, 1756 (1983).
[25] D. J. Evans, J. Chem. Phys. **78**, 3297 (1983).
[26] C. Kittel, *Introduction to Solid State Physics*, 6th ed. (Wiley, Singapore, 1991), p. 118.
[27] A. J. Walton, *Three Phases of Matter*, 2nd ed. (Oxford University Press, 1983), pp. 367–372.
[28] C. J. Twu, MS thesis, National Chung Cheng Univ., Taiwan, 1999.
[29] J. R. Ho, C. J. Twu, and C. C. Hwang, Phys. Rev. B **64**, 014302 (2001).